EQUILIBRIA AND DYNAMICS OF ISOTHERMAL CLOUDS

Chushiro Hayashi
Momoyama Yogoro-cho 1
Fushimi-ku, Kyoto 612
Japan

ABSTRACT. First, equilibrium structure and maximum mass of a rotating isothermal cloud are described. Second, growth rate of fragmentation instability in an infinite disk and filament is presented. Finally, results of 2D and 3D simulations of collapse and fragmentation of rotating isothermal clouds are reviewed and comments are given.

1. INTRODUCTION

Structure and evolution of interstellar clouds have features which are quite different from those of opaque stars. First, the clouds are open systems where the effects of environment such as gravity, pressure, radiation and magnetic field cannot be neglected. Furthermore, mass is not conserved; they experience fragmentation, mass accretion and ejection. Second, they have very diffuse boundaries because they are composed of very soft gases with a polytropic index N ranging from -3 to infinity. Contrary to the case of opaque stars with $N < 3$, the boundaries of clouds are determined by external pressure. Third, in general, clouds have non-spherical structures because they are collapsing, rotating or under the influence of magnetic field. Gravity field in a flattened disk or an elongated cylinder is not so simple as in a sphere. Finally, contrary to the case of opaque stars where we have only to consider evolution through quasi-static equilibria except supernova explosion, we have to taken into account dynamics of clouds such as collapse, fragmentation and even many-body interactions of fragments.

The above features of clouds seem to be too much complicated for us to construct, at present, a consistent theory of evolution and star formation in clouds. We may have to disentangle many factors as described above and for each factor find a simple and precise physical law or theory, from which we can construct a whole theory of evolution.

As examples of such constituent theories, we first review on the equilibrium structure of a rotating isothermal cloud. Compared with a non-rotating case, we have to deal with a problem which has one more

M. Peimbert and J. Jugaku (eds.), Star Forming Regions, 403–416.
© 1987 by the IAU.

https://doi.org/10.1017/S007418090009611X Published online by Cambridge University Press

degree of freedom, i. e., the distribution of specific angular momentum. It is important to know how much mass can be sustained by rotation against gravity. Second, to show the essence of fragmentation condition for a flattened or elongated cloud, the growth rate of instability occurring in an infinite disk and filament will be described. Finally, results of recent numerical simulations of collapse and fragmentation of rotating isothermal clouds will be reviewed. The results will show that fragmentation occurs through formation of a very flattened disk which develops into one or more filaments, in accord with the above simple theory of fragmentation of an infinite disk and filament.

2. EQUILIBRIUM STRUCTURE OF A ROTATING AXISYMMETRIC CLOUD

In order to find an equilibrium structure of an isothermal cloud with mass, M, angular momentum, J, and constant sound velocity, c, we have to impose a boundary condition on the surface of the cloud, contrary to a case with a polytropic index N smaller than 5 where a cloud has a free boundary. Namely, isothermal clouds are subject to the effect of a surrounding medium and, as a simple representation of this effect, here we assume that constant external pressure, P_e, is acting on the cloud surface.

For a rotating cloud, we have to specify the distribution of angular momentum with mass, i. e., a j-m relation. Here, in a cylindrical coordinates (r, ϕ, z) where z denotes the rotation axis, j is a specific angular momentum on the surface of a cylinder with radius r and m is a mass contained inside this cylinder. We adopt here a j-m relation which is the same as in a rigidly-rotating homogeneous sphere. This will be called the standard j-m relation hereafter.

It was shown by Stahler (1983) that equilibrium solutions are specified by the two non-dimensional parameters,

$$P_c/P_e \quad \text{and} \quad \beta_o = 3.36(P_e/c^2)^{1/3}(J/M^{5/3})^2, \tag{1}$$

where P_c is the central pressure and β_o is the ratio of rotational energy to gravitational energy of the above-mentioned sphere. With numerical computations, solutions for $\beta_o \leqq 0.33$ were obtained by Stahler (1983) and, more extensively, those for $\beta_o \leqq 1.31$ by Kiguchi, Narita, Miyama and Hayashi (1986) with results as summarized in the following.

2.1. Mass (M/M_o) - central pressure (P_c/P_e) relation

For the units of pressure and mass, we use P_e and M_o where

$$M_o = c^4/(G^3P_e)^{1/2}, \tag{2}$$

which is nearly equal to the Jeans mass. Relations between M/M_o and P_c/P_e for different values of β_o are shown in Fig. 1. The curve for a well-known non-rotating case ($\beta_o = 0$) has an infinite number of maxima

https://doi.org/10.1017/S007418090009611X Published online by Cambridge University Press

and minima as shown in Fig. 2. In regions above and below this curve, gravity is too large and too small, respectively, for a cloud to be in equilibrium. Namely, the dotted curves in Fig. 2 represent solutions unstable to global contraction and expansion and the first maximum point gives the maximum stable mass, $M = 1.18\ M_o$.

The dashed line in Fig. 1 indicates the position of such maximum stable masses for rotating cases, while the dotted curve denotes a limit such that ring formation occurs in a region above this curve.

It is to be noticed that a rotating axisymmetric cloud with mass as large as 34 M_o can be sustained by centrifugal force against gravity. Furthermore, if isotropic turbulences with velocity v_t exist, all the results are to be modified in such a way that c^2 is replaced by $c^2 + v_t^2$.

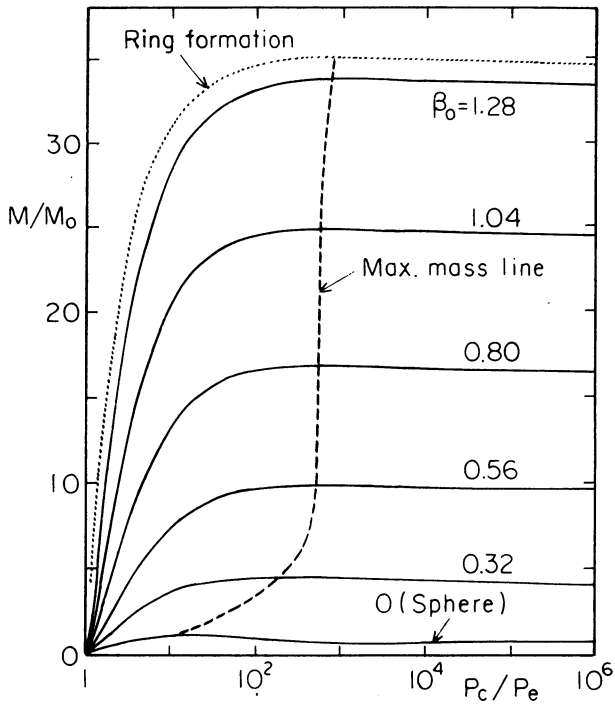

Fig. 1. Mass-central pressure relation for rotating equilibrium clouds.

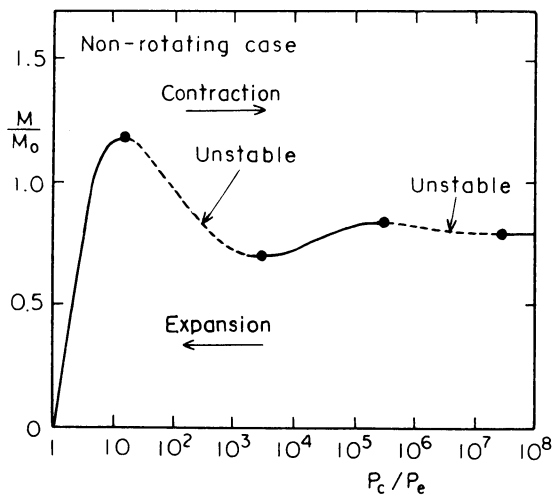

Fig. 2. Mass-central pressure relation for an equilibrium sphere.

2.2. Density distribution and flatness

The equilibrium structure is, in most cases, composed of a small core nearly rigidly rotating and a large envelope which is differentially rotating and has an equatorial density proportional to r^{-2}. However, in a case of $\beta_o > 0.6$, an outermost envelope with nearly uniform density is existing outside the envelope with the above-mentioned density distribution. The ratio of a mean density of a cloud

https://doi.org/10.1017/S007418090009611X Published online by Cambridge University Press

to the boundary density (= P_e/c^2) is always less than 3.8, i. e., the degree of central condensation of mass is small, reflecting the nature of an isothermal gas.

Equi-density contours for a fixed value of P_c/P_e (=100) are shown in Fig. 3. With the increase of β_o (or the total angular momentum, J), the radius, R, increases while the half-thickness in the z-direction is nearly constant. Let the maximum value of z on the cloud surface be denoted by z_{max}. Then, we have approximately

$$z_{max} = 0.3\ c^2/(GP_e)^{1/2}. \tag{3}$$

Now, we define the flatness, f, of the surface by

$$f = R/z_{max}. \tag{4}$$

We find that f is as large as 15 on the critical curve of ring formation shown in Fig. 1. The results are briefly summarized in Table 1.

We can understand the above constancy of z_{max} by considering the half-thickness, z, of an infinite disk with a uniform surface mass density, σ. In this disk, pressure balances with gravity in the z-direction.

For a case where a constant external pressure is acting on this uniform disk, it will be easily found that, with an increase of σ, z first increases, takes a maximum value given by Eq. (3) and decreases afterwards.

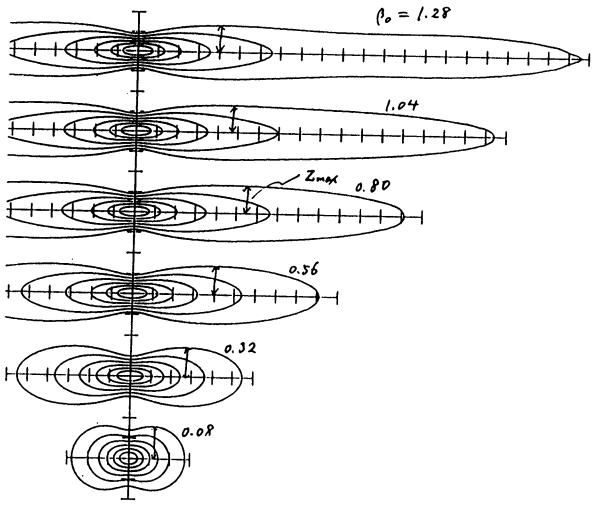

Fig. 3. Equi-density contours in the r-z plane for P_c/P_e = 100.

Table 1. Rotating clouds with maximum masses (<v> is a root mean square velocity averaged with respect to mass).

β_o	0	0.32	1.31
β (= $E_{rot}/\lvert E_{grav}\rvert$)	0	0.30	0.44
$\langle v_{rot}\rangle/c$	0	1.3	2.7
f (= R/z_{max})	1	3.9	16
M/M_o	1.2	4.6	34

https://doi.org/10.1017/S007418090009611X Published online by Cambridge University Press

The above results were obtained by two-dimensional axisymmetric computations and, hence, instability to bar formation has not yet been studied. According to the well-known instability criterion for the Maclaurin spheroid, bar formation is expected to occur in the isothermal cloud if the value of β is greater than 0.27 (see Table 1).

2.3. Remarks

Kiguchi et al.(1986) obtained equilibrium solutions for several j-m relations besides the standard one. Results for a case where j/m is constant is similar to the case of the above standard j-m relation. In cases where, compared with the above two cases, the value of j/m is too large near the center or near the outer boundary, ring formation with a central hole or that with a central core, respectively, was found to occur for a slightly large value of total angular momentum.

Furthermore, they have computed a case where γ of the gas is 2/3, i. e., the polytropic index is -3, considering that the γ value of molecular clouds surrounded by HI regions is about 0.7 (Larson, 1985). They found that equilibrium structure is similar to the isothermal case.

3. FRAGMENTATION OF A UNIFORM DISK AND FILAMENT

Consider the collapse of a triaxial cloud. In general, inequality of the three axes is enlarged with the progress of collapse. First, the shortest axis decreases most rapidly (Zel'dovich 1970) and this decrease is stopped by gas pressure, forming a very flattened disk. The disk begins to fragment as will be shown later but, if the fragmentation is slow, the middle axis of the ellipsoid decreases to form an elongated cylinder which finally fragments. In the following, we consider the growth rate $|\omega|$ of density perturbations, $\delta\rho \propto \exp(i\omega t + i\mathbf{kx})$, as a function of the wave number, $\mathbf{k}$ (see also a review by Larson, 1985).

3.1. An infinite sphere with a uniform density ρ_o

This is the case of well-known Jeans' instability (Jeans 1928) and the dispersion relation for the growth rate is written as

$$\omega^2/4\pi G\rho_o = (k/k_J)^2 - 1, \quad \text{where} \quad k_J = (4\pi G\rho_o)^{1/2}, \tag{5}$$

which shows that the most rapidly growing wavelength is infinite (i. e., k = 0) if the magnitude of initial perturbation is independent of the wavelength. Namely, density contrast is hardly produced in the case of a sphere even if fragmentation occurs.

3.2. An infinite disk with a uniform surface density σ

The dispersion relation was obtained by Goldreich and Lynden-Bell (1965), Elmegreen and Elmegreen (1978), and many others. First we consider a case of zero external pressure. Density distribution in the

https://doi.org/10.1017/S007418090009611X Published online by Cambridge University Press

z-direction in an equilibrium disk is given by

$$\rho(z) = \rho_o \cosh^{-2}(z/z_o), \quad \text{where} \quad z_o = \sigma/2\rho_o \tag{6}$$

is an effective half-thickness of the disk. For a density perturbation of the form

$$\delta\rho \propto e^{i(\omega t + k_x x + k_y y)}, \tag{7}$$

the dispersion relation for a non-rotating disk is expressed in a very good approximation as

$$\omega^2/2\pi G\rho_o = (kz_o)^2 - 2kz_o/(1 + kz_o), \tag{8}$$

where

$$k = (k_x^2 + k_y^2)^{1/2}. \tag{9}$$

In the case of a rotating disk, an additional term representing a tidal effect appears on the right-hand side of Eq. (8) but this term is relatively small, because the centrifugal force should not be too large as to destroy an equilibrium condition assumed for the r-direction.

Exact dispersion relations for isothermal and incompressible fluids are shown in Fig. 4. Contrary to the case of a sphere, the curves have minimum points at finite wavelengths. Namely, for the most rapidly growing mode in the isothermal disk, the value of kz_o is about 0.5 (i. e., the flatness of fragments is about 2π) and the growth time is about z_o/c.

If the external pressure is increased from zero to a large value, the curve for the isothermal case in Fig. 4 approaches that for the incompressible case if we use Eq. (6) for the definition of z_o in terms of the surface density σ and the central density ρ_o of a disk.

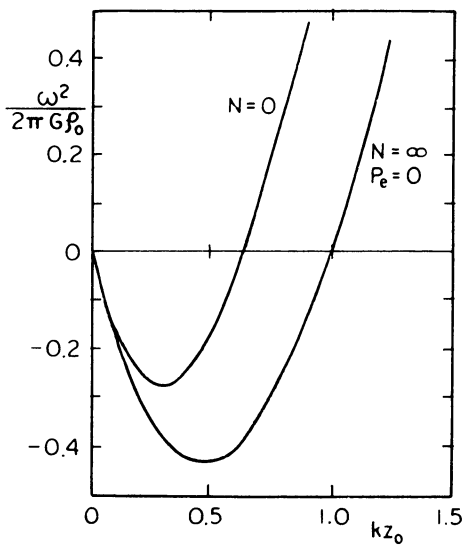

Fig. 4. Dispersion relations for non-rotating disks with polytropic index N = 0 and ∞.

The most rapidly growing mode is degenerate in the **k**-space as shown by Eq.(9). For example, in the case of $k_x = k_y$ we have in the x-y plane a checkered pattern of fragmentation composed of squares. In the case of $k_x = 3k_y$, we have a pattern composed of rectangles with an axial ratio of 3. Recently, non-linear growth of perturbations with

https://doi.org/10.1017/S007418090009611X Published online by Cambridge University Press

such patterns has been numerically simulated by Miyama, Narita and Hayashi (1986). The result shows that in the case of the square pattern each square collapses to form a spheroid, while in the case of the rectangular pattern each rectangle collapses to form a thin filament because of faster contraction of a shorter axis.

Now, we consider a statistical problem as to the **k**-dependence of initial perturbation. If we assume that the magnitude of initial density perturbations is uniform in the **k**-space, the probability of forming square-like patterns is much lower than that of rectangular patterns. Namely, in view of the result of non-linear growth, formation of thin filaments is much more probable than that of roundish spheroids. Furthermore, it is to be noticed that the mass of a square is smaller than that of a rectangle and that the peak of the growth rate shown in Fig. 4 is not so sharp but broad. These features will be important in studying the mass spectrum of star formation.

3.3. An infinite cylinder with a uniform line mass density M_L

We consider a circular cylinder which extends to infinity in the z-direction. In equilibrium, gas pressure balances with gravity in the r-direction and in the case of zero external pressure we have for the density distribution and the line mass density

$$\rho(r) = \rho_o/(1 + r^2/a^2)^2, \tag{10}$$

$$M_L = 2\pi\int_0^\infty \rho(r) r dr = 2c^2/G, \tag{11}$$

where

$$a = (M_L/\pi\rho_o)^{1/2}, \tag{12}$$

is an effective radius of the cylinder. In the case of $P_e = 0$, the line mass takes a maximum value given by Eq. (11). This is a characteristic of an isothermal filament which is similar to an equilibrium of a polytropic sphere with N = 3, where Chandrasekhar's limiting mass exists.

Now, we consider a density perturbation of the form

$$\delta\rho \propto e^{i(\omega t + kz + m\phi)}. \tag{13}$$

The mode for m = 1 is a kink which is always stable and here we consider only a sausage-type instability corresponding to m = 0. Dispersion

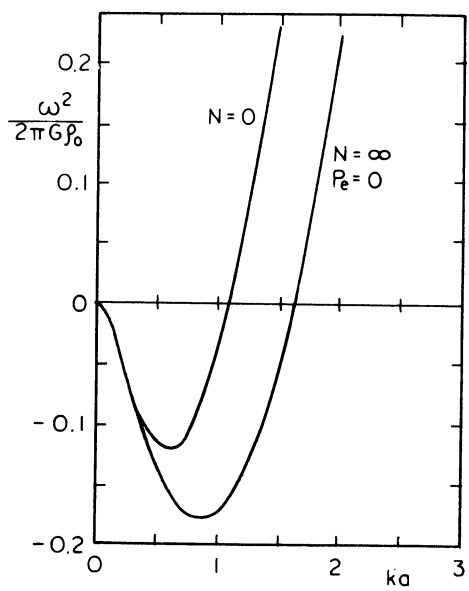

Fig. 5. Dispersion relation for a non-rotating cylinder.

https://doi.org/10.1017/S007418090009611X Published online by Cambridge University Press

relations for an isothermal as well as incompressible cylinder are shown in Fig. 5. The most rapidly growing mode has a wave-length (= $2\pi/k$) of about $2\pi a$, a flatness of about 2π and a growth time of about a/c.

In a case where external pressure is acting on the surface of a cylinder, the curve for an isothermal cylinder in Fig. 5 approaches that for incompressible one with the increase of the external pressure, as it should be. Furthermore, in a large wave-length limit, $ka \to 0$, both of the curves in Fig. 5 are expressed in the form

$$|\omega^2|/2\pi G\rho_o = (ka)^2 \log(ka/2). \tag{14}$$

It is to be noticed that the right-hand side of Eq. (14) is equal to 2 and $2kz_o$ in the cases of a sphere and a disk, respectively, as will be seen in Eqs. (5) and (8). This means that, in the case of a cylinder, the growth of perturbations with large wave-lengths is much slower than in the case of a disk and, accordingly, density contrast is more easily produced by fragmentation.

In conclusion, if a very thin disk or filament is formed, it soon fragments into a number of small clouds with flatness of about 2π (see Eq.(4) for the definition of flatness). The main reason for this is that the total gravitational energy of a system is greatly reduced by such fragmentation.

4. COLLAPSE AND FRAGMENTATION OF A ROTATING ISOTHERMAL CLOUD

Dynamics of a cloud is a problem more complicated than eouilibrium of a cloud since it contains one more degree of freedom, i. e., it depends on the initial density distribution besides the j-m relation as mentioned in Section 2. On the collapse of a rotating isothermal cloud, a great number of numerical 2D and 3D computations have been made since Larson (1972) started his 2D computation. As for the initial condition of a cloud, a homogeneous rigidly-rotating sphere has been adopted in most of the computations. For papers before 1980, see a review by Bodenheimer (1981) and, as the later papers until now, see Boss and Harber (1982), Wood (1982), Narita, McNally, Pearce and Sørensen (1983), Miyama, Hayashi and Narita (1984), and Narita, Hayashi and Miyama (1984).

In the above computations, results for the same initial condition were not always in agreement with each other. This seems to be due to mathematical errors including, for example, an artificial transport of angular momentum. It was difficult, especially in early days, to eliminate such errors and there remained questions as to precise conditions for ring formation, central runaway and fragmentation.

In the following, we will summarize mainly the recent results of Miyama et al.(1984) and Narita et al. (1984), who have provided answers to the above questions by using, respectively, two different numerical

https://doi.org/10.1017/S007418090009611X Published online by Cambridge University Press

methods, i. e., (1) a Lagrangian "Smoothed-Particle Method" with 1000 - 4000 particles representing spherical equal-mass fluid elements with Gaussian density distributions and (2) an Eulerian "Fluid-In-Cell Method" with 10^4 Lagrangian test particles to prevent the artificial transport of angular momentum. They adopted for initial condition a homogeneous rigidly-rotating sphere, which is specified by the two non-dimensional parameters

$$\alpha = E_{th}/|E_{grav}| \quad \text{and} \quad \beta = E_{rot}/|E_{grav}|. \tag{15}$$

It is to be noticed that the product, $\alpha\beta$, is independent of the cloud size and written in the form

$$\alpha\beta = (125/24)(cJ/GM^2)^2, \tag{16}$$

which means that $\alpha\beta$ is a conserved quantity during collapse if the transport of angular momentum is negligible, i. e., if the effects of viscosity and also departure from axisymmetry can be neglected.

4.1. Results of Miyama et al. with the Smoothed-Particle method

Miyama et al. (1984) made 3D computations of collapse for initial conditions with 17 different sets of (α, β) values, initial density fluctuations being smaller than 5 per cent. Computations were stopped at $t = 2 - 3\ t_{ff}$, where a maximum density in a cloud became 10^4 times the initial density. As a result they found that the characteristic of dynamics is determined by one parameter, $\alpha\beta$, and all the 17 cases are grouped into the following 3 classes. This classification is consistent with the results of computation by Wood (1982).

1. $\alpha\beta \geqq 0.20$ (no collapse). A cloud begins to expand after slight contraction and, afterwards, oscillates around an equilibrium state as described in Section 2.

2. $0.20 > \alpha\beta \geqq 0.12$ (collapse without fragmentation). A cloud first collapses in the z-direction and this is stopped by the increase of gas pressure. Then a central part of the cloud collapses in the r-direction and bounces weakly with a subsonic velocity, forming a flat disk. This disk is not so flattened (the flatness being less than 8) as to be able to fragment and begins to collapse again. The gas remaining in the outer region with a large part of the total mass is nearly in equilibrium and has a density distribution proportional to r^{-2} and an angular velocity distribution proportional to r^{-1}. Afterwards, collapse of the disk will be stopped by gas pressure when it will become opaque to form a stellar core. Finally a single star will be formed by accretion of the remaining gas onto the core.

3. $0.12 > \alpha\beta$ (collapse and fragmentation). After collapse in the z-direction, a central part of a cloud collapses in the r-direction and then bounces strongly with a supersonic velocity, forming a very flat disk containing about 30 per cent of the total mass. The disk soon de-

https://doi.org/10.1017/S007418090009611X Published online by Cambridge University Press

velops into one or more filaments and each filament finally fragments into small clouds, in accordance with the fragmentation condition described in Section 3. It was found that in a case where $\alpha\beta$ is smaller the disk has a greater flatness and the number of fragments is larger. For example, in a case with $\alpha = 0.4$ and $\beta = 0.3$, the disk has a flatness of about 7 and it develops into a S-shaped filament (Fig. 6) which finally fragments into 3 clouds. On the other hand, in a case with $\alpha = 0.2$ and $\beta = 0.3$, the disk has a flatness as large as 14 and develops into multi-armed filaments (Fig. 7), which finally fragment into 8 pieces. The above fragments are interacting gravitationally with each other and it is expected that, through virialization and sticking as well as accretion of the remaining gas, finally double stars or triple stars will be formed.

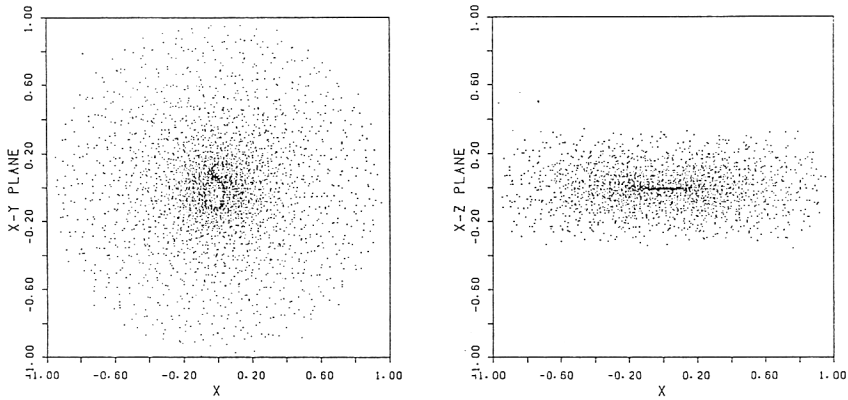

Fig. 6. Projections of particles on equatorial and meridional planes at a stage immediately before fragmentation for a case of $\alpha = 0.4$ and $\beta = 0.3$.

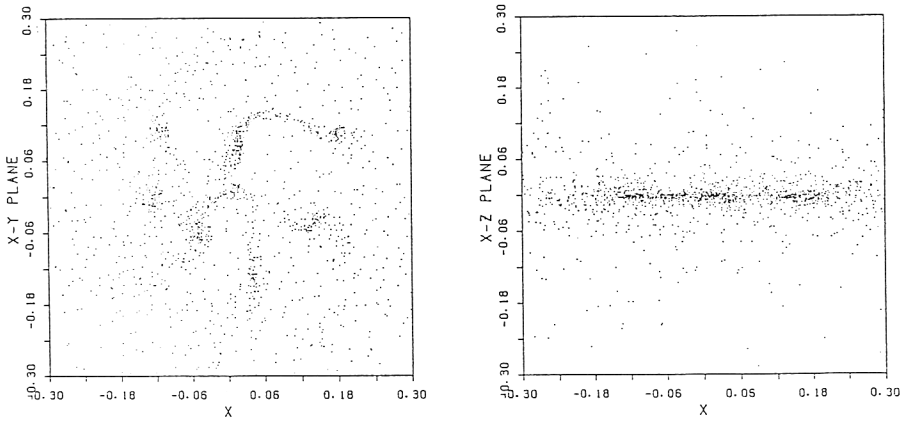

Fig. 7. The same as in Fig. 6 for a case of $\alpha = 0.2$ and $\beta = 0.3$.

https://doi.org/10.1017/S007418090009611X Published online by Cambridge University Press

4.2. Results of Narita et al. with the Fluid-In-Cell method

In order to solve a runaway problem on the collapse of the center of a cloud and also to clarify the mechanism of bounce forming a flat disk as mentioned in Section 4.1, Narita et al. (1984) performed 2D computations of collapse together with 1D computations using a thin-disk approximation. As to initial condition, besides the case of a sphere they took into account a case of a rigidly-rotating disk which is already in equilibrium in the z-direction.

As a result they found that, for almost all of plausible initial conditions (i. e., except for cases of a sphere with $\alpha < 0.1$), collapse proceeds with such a structure as composed of the three parts:

(1) a rigidly-rotating homogeneous core with a flatness between 4 and 6 and with a radius, a_c, which decreases continuously with time,

(2) an inner envelope which has nearly the same flatness as the core and distributions of density, surface density and angular velocity proportional to r^{-2}, r^{-1} and r^{-1}, respectively, and

(3) an outer envelope with a structure depending upon the details of initial condition in the surface region.

The time variation of surface density in the core and in the inner envelope is schematically shown in Fig. 8. The relation, $\sigma \propto r^{-1}$, holding in the inner envelope results from a balance of gravity and gas pressure, reflecting the nature of an isothermal cloud. The surface density of the core, σ_c, increases with time as

$$\sigma_c(t)a_c(t) = \text{constant}. \qquad (17)$$

Namely, with the decrease of the core radius, a_c, the central density tends to infinity as a_c^{-2}. This central runaway was first found by Norman, Wilson and Barton (1980). It is to be noticed that the core mass, $\pi\sigma_c a_c^2$, is proportional to a_c and it is always of the order of Jeans' mass.

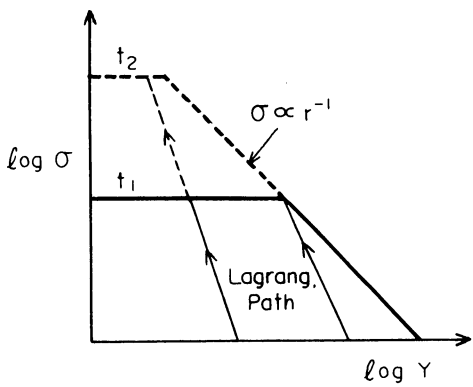

Fig. 8. Distribution of surface density in the core and the inner envelope at two times t_1 and t_2. The thin lines denotes Lagrangian paths.

The reason for why the above runaway occurs instead of a centrifugal bounce will be understood in the following way. Let us consider motion of a Lagrangian fluid element in the core, $r = r(t)$, which is lying on a cylindrical surface with a fixed interior mass, m, i. e.,

$$m = \pi\sigma_c(t)r^2(t). \qquad (18)$$

https://doi.org/10.1017/S007418090009611X Published online by Cambridge University Press

In the case of a flattened core considered, gravity acting on the element is written in the form

$$F_{grav} = -k(Gm/r^2)(r/a_c) \quad \text{for} \quad r/a_c < 1, \tag{19}$$

where k is a constant of the order of unity. On the other hand, centrifugal force is given by

$$F_{cent} = j^2/r^3, \tag{20}$$

where the specific angular momentum, j, is proportional to m, according to the initial condition. From Eqs. (19) and (20) we have

$$|F_{cent}/F_{grav}| = \text{constant} \times a_c(t)\sigma_c(t), \tag{21}$$

which is constant according to Eq. (17) and always less than unity if initially less than unity, i. e., if a cloud does begin collapsing.

Narita et al. showed that the central runaway occurs in cases where γ of the gas is equal to or less than unity, while bounce occurs at a finite central density in cases where $\gamma > 1$. In reality, the core becomes opaque to thermal radiation at a density of about 10^{-13} g/cm^3 and γ changes to a value of about 1.4. As a result, the core stops contraction and the gas exterior to the core forms a very flat disk rotating around the core. Gravity of this disk acts on the core to expand it in the r-direction and this is a mechanism of central bounce in the collapse of a rotating "isothermal" cloud. Indeed, in the 3D computations by Miyama et al. described in Section 4.1, they used an equation of state such that γ changes into 4/3 when the density becomes greater than 10^4 times the initial density.

4.3. Remarks on the fragments of a cloud

4.3.1. **Reduction of spin angular momentum.** The 3D computations by Miyama et al., as described in Section 4.2, show that each fragment of a cloud has spin angular momentum which is smaller than orbital angular momentum by a factor of 10 to 20. This indicates that fragmentation is a very efficient process for conversion of spin into orbital angular momentum, as was pointed out by Boss and Bodenheimer (1979) and Bodenheimer, Tohline and Black (1980).

4.3.2. **Refragmentation of a fragment.** Miyama et al. found in their 3D computations that, in the case of fragmentation into three clouds with masses of about one tenth of a parent cloud, the initial value of $\alpha\beta$ is 0.12 while the $\alpha\beta$ value of each fragment is about 0.02. Note that, as shown by Eq.(16), $\alpha\beta$ is conserved during collapse but changed by fragmentation. Now, let us consider a very flat disk just before fragmentation, which is rotating with supersonic velocities. From a condition that gravity balances with gas pressure in the z-direction and gravity balances with centrifugal force in the r-direction in the disk, we obtain the following approximate formulas for the rotation velocity,

https://doi.org/10.1017/S007418090009611X Published online by Cambridge University Press

v_{rot}, the radius, R, the half-thickness, z, and the mean density, ρ, of the disk.

$$\langle v_{rot}^2 \rangle \simeq c^2(\alpha\beta)^{-1}, \quad R \simeq (GM/c^2)\alpha\beta, \tag{22}$$

$$z \simeq (GM/c^2)(\alpha\beta)^2, \quad \text{and} \quad \rho \simeq (c^6/G^3M^2)(\alpha\beta)^{-4}. \tag{23}$$

For the above-mentioned values of $\alpha\beta$, we can expect from Eq. (23) that the second fragmentation occurs when the mean density of a fragment becomes 10^4 times the density just before the first fragmentation. This means that, if a parent cloud starts collapsing at a density of 10^{-20} g/cm^3, refragmentation may occur once or twice before fragments become almost completely opaque.

4.3.3. **Minimum mass of a fragment and formation of a stellar core.** If the last fragmentation occurs at a density of 10^{-13} g/cm^3, mass of a fragment is of the order of Jeans' mass for this density, i. e., the mass of Jupiter. The fragment mass is smaller if the last fragmentation occurs at higher densities. Anyhow, the total mass of all the fragments may be of the order of 1/10 of the original cloud. These fragments will interacts gravitationally with each other and, through scattering (i.e., virialization) and accumulation, they will finally form a stellar core, onto which the remaining gas is accreting relatively slowly.

5. CONCLUSION

In the above, we have reviewed recent studies of equilibrium structure, dynamical collapse and also fragmentation of rotating isothermal clouds, which are under a simplified environment condition that constant external pressure is acting on the cloud surface. It has been shown that rotating clouds have features very different from non-rotating spherical clouds. For example, rotation can sustain a cloud with mass much greater than that of a spherical cloud. Non-spherical collapse with rotation gives rise to a flattened disk and, in a case of a very flattened disk, it forms one or more filaments which soon fragment into a number of small clouds. In order to understand these features, we have to notice that gravity field in a very flattened disk is considerably different from that in a spheroidal configuration with internal equi-density surfaces as given by similar spheroids and it rather resembles that in a toroidal configuration where gravity of matter existing in exterior regions cannot be neglected.

We have neglected the effect of magnetic field, which will be important in understanding various evolutionary processes occurring in interstellar clouds until the formation of pre-main-sequence stars. However, our present knowledge on this effect is very limited, especially for clouds with internal shear motion, e. g., differentially rotating clouds. Furthermore, there is a problem on the boundary condition for magnetic field; when clouds are interacting with neighboring clouds through rapid propagation of Alfvén waves in a tenuous intercloud medium

https://doi.org/10.1017/S007418090009611X Published online by Cambridge University Press

we may have to deal with a many-body problem if the magnetic interactions are too strong. In other words, for a cloud with internal and external shear motion, we have to solve difficult but important problems as to amplification and dissipation (i. e., decay and reconnection) of magnetic fields.

REFERENCES

Bodenheimer, P. 1981, in IAU Symposium 93, Fundamental Problems in the Theory of Stellar Evolution, ed. D. Sugimoto, D. Q. Lamb and D. N. Schramm (Dordrecht, Reidel), p. 5.
Bodenheimer, P., Tohline, J. E., and Black, D. C. 1980, Ap. J., **242**, 209.
Boss, A. P., and Bodenheimer, P. 1979, Ap. J., **234**, 289.
Boss, A. P., and Harber, J. G. 1982, Ap. J., **255**, 240.
Elmegreen, B. G., and Elmegreen D. M. 1978, Ap. J., **220**, 1051.
Goldreich, P., and Lynden-Bell, D. 1965, M. N. R. A. S., **130**, 7.
Jeans, J. H. 1928, Astronomy and Cosmogony (Cambridge University Press, Cambridge).
Kiguchi, M., Narita, S., Miyama, S. M., and Hayashi, C. 1986, to be published.
Larson, R. B. 1972, M. N. R. A. S., **156**, 437.
Larson, R. B. 1985, M. N. R. A. S., **214**, 379.
Miyama, S. M., Hayashi, C., and Narita, S. 1984, Ap. J., **279**, 621.
Miyama, S. M., Hayashi, C., and Narita, S. 1986, to be published.
Narita, s., McNally, D., Pearce, G. L., and Sørensen, S. A. 1983, M. N. R. A. S., **203**, 491.
Narita, S., Hayashi, C., and Miyama, S. M. 1984, Prog. Theor. Phys., **72**, 1118.
Norman, M. L., Wilson, J. R., and Barton, R. T. 1980, Ap. J., **239**, 968.
Stahler, S. W. 1983, Ap. J., **268**, 155 and 165.
Wood, D. 1982, M. N. R. A. S., **199**, 331.
Zel'dovich, Ya. B. 1970, Astr. Astrophys., **5**, 84.

SHU: What is the fraction of total mass which ends up in fragments? My impression is that it is fairly large, and therefore this picture predicts a fairly large star formation efficiency. Is this correct?

HAYASHI: The results of the 3D simulation show that the fragments as a whole contain 20-30% of the total mass. It seems difficult to decrease this percentage by orders of magnitude by adopting different initial conditions. However, if we take into account the re-fragmentation of each fragment, the above percentage will be reduced by a factor of about 5.

https://doi.org/10.1017/S007418090009611X Published online by Cambridge University Press